DELPHI Collaboration

DELPHI 2000-099 CONF 398
30 June, 2000

Search for Spontaneous R-parity violation at $\sqrt{s} =$ 183 GeV and 189 GeV

D. Moraes, L. de Paula and M. Gandelman
Instituto de Física - LAPE/UFRJ - Brasil

Abstract

Searches for spontaneous R-parity violating signals at $\sqrt{s} = 183$ GeV and $\sqrt{s} = 189$ GeV have been performed using the 1997 and 1998 DELPHI data, under the assumption of R-parity breaking in the third lepton family. The expected topology for the decay of a pair of charginos into two acoplanar taus plus missing energy showed no evidence for a signal. The results provide limits on the chargino mass and MSSM parameter space.

Contributed Paper for ICHEP2000

1 Introduction

R-parity is a discrete symmetry assigned as $R_p = (-1)^{3B+L+2S}$, where B is the baryon number, L is the lepton number and S is the particle spin. In the Minimal Supersymmetric Standard Model (MSSM) the R-parity symmetry is assumed to be conserved [1]. Under this assumption the supersymmetric particles must be produced in pairs, every SUSY particle decays into another SUSY particle and the lightest of them is absolutely stable. These features underly most of the experimental searches for supersymmetric states.

One alternative supersymmetric scenario is to consider the R-parity as an exact Lagrangian symmetry, broken spontaneously through the Higgs mechanism [2]. This may take place via non-zero vacuum expectation values (VEVs) for scalar neutrinos, such as for the right and left handed stau neutrinos

$$v_R = \langle \tilde{\nu}_{R\tau} \rangle \ ; \quad v_L = \langle \tilde{\nu}_{L\tau} \rangle \ . \tag{1}$$

In this case there are two main scenarios depending on whether the lepton number is a gauge symmetry or not [3, 4, 5, 6, 7]. In the absence of an additional gauge symmetry, it leads to the existence of a physical massless Nambu-Goldstone boson, called Majoron (J) [4]. In this context the Majoron remains massless and therefore stable, if there are no explicit R-parity violating terms.

1.1 Spontaneous R-Parity violation

In the present work we consider the simplest version of the R-parity spontaneous violation model described in Ref. [4, 5]. In this model the Lagrangian is specified by the superpotential

$$W = W_1 + h_\nu \nu^c L \mathbf{H}_u + h \Phi \nu^c \mathbf{S} + h.c. \tag{2}$$

that conserves the total lepton number and R-parity. The first part of this equation contains the basic MSSM superpotential terms, including an isosinglet scalar Φ with a linear superpotential coupling, written as:

$$W_1 = h_u Q u^c \mathbf{H}_u + h_d Q d^c \mathbf{H}_d + h_e e^c L \mathbf{H}_d + (h_0 \mathbf{H}_u H_d - \mu'^2)\Phi \ . \tag{3}$$

The couplings h_u, h_d, h_e, h_ν, h_0, h are described by arbitrary matrices in the generation space which explicitly break flavour conservation. The additional chiral superfields ν^c, S [8] and Φ [9] are singlets under $SU(2) \bigotimes U(1)$ and carry a conserved lepton number assigned as -1, 1 and 0, respectively. These superfields may induce the spontaneous violation of R-parity, given by the imaginary part of:

$$\frac{v_L^2}{V v^2}(v_u H_u - v_d H_d) + \frac{v_L}{V}\tilde{\nu}_\tau - \frac{v_R}{V}\tilde{\nu}_\tau^c + \frac{v_S}{V}\tilde{S}_\tau \ , \tag{4}$$

leading to an R-odd Majoron. The isosinglet VEVs $v_R = \langle \tilde{\nu}_{R\tau} \rangle$ and $v_S = \langle \tilde{S}_\tau \rangle$, with $V = \sqrt{v_R^2 + v_S^2}$, characterize the R-parity breaking and the isodoublet VEVs $v_u = \langle H_u \rangle$, $v_d = \langle H_d \rangle$ and $v_L = \langle \tilde{\nu}_{L\tau} \rangle$ induce the electroweak breaking and generate the fermion masses. For theoretical reasons the R-parity breaking was introduced only in the third family, since the largest Yukawa couplings are those of the third generation. In that case

the R-parity breaking is effectively parameterized by a bilinear superpotential term given by:

$$\epsilon_i \equiv h_{\nu_{i3}} v_{R3} \ . \tag{5}$$

This effective parameter leads to the R-parity violating gauge couplings and contributes to the mixing between the charged (neutral) leptons and the charginos (neutralinos), as can be seen from the fermion mass matrices in Ref. [10].

By construction, neutrinos are massless at the Lagrangian level but get mass from the mixing with neutralinos [6, 10]. As a result, all R-parity violating observables are directly correlated to the τ neutrino mass:

$$m_{\nu_\tau} \sim \frac{\xi \epsilon^2}{m_{\tilde{\chi}}} \ , \tag{6}$$

where $m_{\tilde{\chi}}$ is the neutralino mass, ϵ is the R-parity violation parameter and ξ is an effective parameter [11] given as a function of M_2, μ and $\tan\beta$.

1.2 Chargino Decay Modes

At LEP2 the chargino can be pair produced from e^+e^- via exchange of $\gamma, \mathrm{Z}, \tilde{\nu}$. In the present analysis it is assumed that all sfermions are sufficiently heavy ($\mathrm{M}_{\tilde{\nu}} \geq 300\,\mathrm{GeV/c^2}$) not to influence the chargino production or decay. Therefore, only the γ and Z s-channels contribute to the chargino cross-section. In the spontaneous R-parity violation model with R-parity breaking in the third generation the lightest chargino ($\tilde{\chi}^\pm$) can undergo a two-body decay mode

$$\tilde{\chi}^\pm \rightarrow \tau^\pm J \tag{7}$$

in addition to the "conventional" chargino channels

$$\tilde{\chi}^\pm \rightarrow \nu_\tau \mathrm{W}^\pm \rightarrow \nu_\tau \mathrm{q}\bar{\mathrm{q}}', \ \nu_\tau \mathrm{l}_\mathrm{i}^\pm \nu_\mathrm{i} \tag{8}$$

and

$$\tilde{\chi}^\pm \rightarrow \tilde{\chi}^0 \mathrm{W}^\pm \rightarrow \tilde{\chi}^0 \mathrm{q}\bar{\mathrm{q}}', \ \tilde{\chi}^0 \mathrm{l}_\mathrm{i}^\pm \nu_\mathrm{i} \ . \tag{9}$$

Both two-body decay (7) and the decay with neutralino in the final state (9) are R-parity conserving, while in equation (8) the chargino decays through an R-parity violating vertex. The decay branching ratios depend strongly on the effective violation parameter (ϵ), as can be observed in figure 1. Note that in a large range of ϵ the new two-body decay mode is the dominant channel and, since it is R-parity conserving, it can be large.

1.3 Parameters Values

All the results discussed in the following sections were achieved by assuming that the chargino always decays via the new two body decay mode, described in equation (7). As was already mentioned, all sfermions are considered to be sufficiently heavy ($\mathrm{M}_{\tilde{\nu}} \geq 300\,\mathrm{GeV/c^2}$) not to influence the chargino production or decay. Typical ranges of values for the SUSY parameters $\mu \equiv h_0 \langle \Phi \rangle$ and M_2 are assumed:

$$-200\,\mathrm{GeV/c^2} \leq \mu \leq 200\,\mathrm{GeV/c^2} \tag{10}$$

$$40\,\mathrm{GeV/c^2} \leq \mathrm{M}_2 \leq 400\,\mathrm{GeV/c^2} \ , \tag{11}$$

which account for the chargino production within the kinematical reach of LEP. Also assumed are the GUT relation $M_1/M_2 = 5/3 \tan^2\theta_W$ and that $\tan\beta$ lies in the range

$$2 \leq \tan\beta = \frac{v_u}{v_d} \leq 40 \ . \tag{12}$$

2 Detector Description

The following is a summary of the properties of the DELPHI detector [12] relevant to this analysis. Charged particle tracks were reconstructed in the 1.2 T solenoidal magnetic field by a system of cylindrical tracking chambers. These were the microvertex Detector (VD), the Inner Detector (ID), the Time Projection Chamber (TPC), and the Outer Detector (OD). In addition, two planes of drift chambers aligned perpendicular to the beam axis (Forward Chambers A and B) tracked particles in the forward and backward directions, covering polar angles $11^\circ < \theta < 33^\circ$ and $147^\circ < \theta < 169^\circ$ with respect to the beam (z) direction.

The VD consisted of three cylindrical layers of silicon detectors, at radii 6.3 cm, 9.0 cm and 11.0 cm. All three layers measured coordinates in the plane transverse to the beam. The closest (6.3 cm) and the outer (11.0 cm) layers contained double-sided detectors to measure also z coordinates. The polar angle coverage of the VD was from 25° to 155° for the closest and from 44° to 136° for the outer layer. Mini-strips and pixel detectors making up the Very Forward Tracker (VFT) have been added to the ends of the VD increasing the angular acceptance to between 10° and 25°. The ID was a cylindrical drift chamber (inner radius 12 cm and outer radius 22 cm) covering polar angles between 15° and 165°. The TPC, the principal tracking device of DELPHI, was a cylinder of 30 cm inner radius, 122 cm outer radius and had a length of 2.7 m. Each end-plate was divided into 6 sectors, with 192 sense wires used for the dE/dx measurement and 16 circular pad rows used for 3 dimensional space-point reconstruction. The OD consisted of 5 layers of drift cells at radii between 192 cm and 208 cm, covering polar angles between 43° and 137°.

The average momentum resolution for the charged particles in hadronic final states was in the range $\Delta p/p^2 \simeq 0.001$ to 0.01 $(\mathrm{GeV/c})^{-1}$, depending on which detectors were used in the track fit [12].

The electromagnetic calorimeters were the High density Projection Chamber (HPC) covering the barrel region of $40^\circ < \theta < 140^\circ$, the Forward ElectroMagnetic Calorimeter (FEMC) covering $11^\circ < \theta < 36^\circ$ and $144^\circ < \theta < 169^\circ$, and the STIC, a Scintillator TIle Calorimeter which extended coverage down to 1.66° from the beam axis in either direction. The 40° taggers were a series of single layer scintillator-lead counters used to veto electromagnetic particles that would otherwise have been missed in the region between the HPC and FEMC. A similar set of taggers was arranged at 90° to cover the gap between the two halves of the HPC. The efficiency to register a photon with energy above 5 GeV measured with the LEP1 data was above 99%. The hadron calorimeter (HCAL) covered 98% of the solid angle. Muons with momenta above 2 GeV penetrated the HCAL and were recorded in a set of muon drift chambers.

3 Data Samples

The data collected by the DELPHI detector during 1997 at $\sqrt{s} \simeq 183\,\mathrm{GeV}$ and 1998 at $\sqrt{s} \simeq 189\,\mathrm{GeV}$, corresponding to an integrated luminosity of $53\,\mathrm{pb}^{-1}$ and $158\,\mathrm{pb}^{-1}$ respectively, were analysed.

To evaluate background contaminations, different contributions from the Standard Model processes were considered. The background processes WW, Weν_e, ZZ, Ze$^+e^-$ and $\mathrm{Z}/\gamma \rightarrow q\bar{q}(\gamma)$ were generated using PYTHIA [13], while the events $\mathrm{Z}/\gamma \rightarrow \tau^+\tau^-(\gamma), \mu^+\mu^-(\gamma)$ were produced by KORALZ [14] and DYMU3 [15] respectively. A cross-check was performed using the four-fermion final states generated with EXCALIBUR [16]. The generator BABAMC [17] was used for the Bhabha scattering. Two-photon interactions leading to leptonic and hadronic final states were produced by the BDK [18] and TWOGAM [19] programs, respectively. All the background events were passed through a detailed detector response simulation (DELSIM) and reconstructed as the real data [12].

The program RP-generator II, described in reference [5], was used to calculate masses, cross-sections and branching ratios of the chargino production and its corresponding decays. The chargino pair production was considered for different values of the R-parity violation parameter (ϵ) and at several points of the MSSM parameter space ($\tan\beta, \mu, \mathrm{M}_2$). For the signal, a faster simulation program SGV[1] was used to check the points that were not generated by the full DELPHI simulation program (DELSIM). The SGV program does not simulate the DELPHI taggers. To correct for this effect, ten chargino mass points, with 1000 events each, were simulated by DELSIM and the selection efficiency[2] of the programs were compared. This procedure was done for the 183 GeV analysis and the correction factors for the SGV efficiency if the taggers are considered, shown in figure 2, were also used for the 189 GeV simulation.

4 Chargino Searches

With the R-parity spontaneous breaking, the chargino can decay through an R-parity conserving vertex into $\tau^{\pm}J$ events. Due to the undetectable Majoron, such events have the topology of two taus acoplanar with the beam axis plus missing energy. To select events with this signature it was required that there were two clusters of well reconstructed charged and neutral particles each cluster with invariant mass below $5.5\,\mathrm{GeV/c^2}$; events have less than 7 charged particles and a total momentum transverse to the beam greater than 4 GeV/c. Charged and neutral particles were considered as well reconstructed if their momenta were between 1 GeV/c and the beam momentum and their polar angles were between 30° and 150°. The clusters were constructed by considering all combinations of assigning the charged particles in the event into two groups. Neutral particles were then added to the groups such that the mass remains below the cut value and a neutral that can not be added to either of the two groups is considered as isolated.

Events with forward going secondaries were avoided by rejecting any with energy

[1] The program "Simulation a Grande Vitesse" (SGV) is described in http://delphiwww.cern.ch/~berggren/sgv.html

[2] The efficiency of the chargino selection is defined as the number of events satisfying the cuts defined in Secion 4.1 divided by the total number of generated chargino events.

measured in a 30° cone around the beam axis. Events were also rejected if there were signals in the 90° or 40° taggers.

4.1 Event Selection at 183 GeV

The events were selected requiring an acoplanarity[3] between 4° and 175°. To reject the radiative return to the Z background, no events with isolated photons with more than 5 GeV were accepted. The $\gamma\gamma$ and $\mu^+\mu^-(\gamma)$ backgrounds were reduced by requiring that the events had at least one charged particle with momentum between 5 GeV/c and 60 GeV/c. To reduce the $\tau^+\tau^-(\gamma)$ background the square of transverse momentum with respect to the thrust axis divided by the thrust had to be above 0.75 $(\mathrm{GeV/c})^2$.

To reduce the $\gamma\gamma$ background further, events with momentum of their most energetic charged particle (P_{max}) below 10 GeV/c had to have total momentum transverse to the beam above 10.5 GeV/c. For events with $P_{max} > 10$ GeV/c, the main remaining contamination comes from $\mathrm{Z}/\gamma \to \tau^+\tau^-$ and WW. For those, if the acoplanarity was below 165°, the angle between the missing momentum and the beam had to be greater than 30°. On the other hand, if the acoplanarity was above 165°, it was required that the momentum of the most energetic lepton was below 23.5 GeV/c and the angle between the missing momentum and the beam was greater than 34.5°.

Figures 3a and 3b show the agreement between data and simulated background events after a preliminary selection, while figure 4a shows the dependence of the signal detection efficiency on the chargino mass. The selection criteria result in a detection efficiency of around 22 %.

4.2 Event Selection at 189 GeV

LEP delivered a higher luminosity for this energy and tighter cuts were applied. The required acoplanarity had to be between 4° and 170° and no events with an isolated photon were accepted. The momentum of each of the two particle clusters had to be above 5 GeV/c and below 55 GeV/c and the square of transverse momentum with respect to the thrust axis divided by the thrust had to be above 1.0 $(\mathrm{GeV/c})^2$. All the events had to have the angle between the missing momentum and the beam greater than 35°.

The events from radiative return to the Z and WW processes were mainly rejected by requiring a total momentum transverse to the beam greater than 9 GeV/c and the momentum of the most energetic lepton below 23 GeV/c.

If one cluster had a momentum above 10 GeV/c and the acoplanarity was below 165° it was also required that the value of the effective centre-of-mass energy after any initial state radiation ($\sqrt{s'}$) [20] did not fall in the region between 90 GeV and 94 GeV. For an acoplanarity greater than 165°, the angle between the missing momentum and the beam was required to be greater than 40° and the visible mass lower than 70 $\mathrm{GeV/c^2}$. This last cut is very efficient at removing the WW background.

Figure 3c and 3d show the agreement between data and simulated background events after a preliminary selection, while figure 4b shows the dependence of the signal detection efficiency on the chargino mass. The selection criteria result in a detection efficiency of around 17 %.

[3]The acoplanarity is defined as the magnitude of the angle between the jets when projected onto the plane perpendicular to the beam.

5 Results

As a result of the selection procedure, 6 candidates of $\tilde{\chi}^{\pm} \to \tau^{\pm} + J$ were selected at 183 GeV, with a background estimation of 6.28 ± 0.40. At 189 GeV, 9 candidates were found, with an expected background of 9.55 ± 0.44. Table 1 summarises the number of accepted events in the data, together the predicted number of events from background sources. The systematic and statistical errors on the simulated background calculation are insignificant compared to the experimental statistical accuracy.

Assuming the chargino decays exclusively to $\tau^{\pm}J$, the combined data for 183 GeV and 189 GeV were used to obtain the minimal excluded cross-section given by the standard formula in [21] and the chargino mass limit; both are shown in figure 5. The excluded domains of the MSSM parameter space for $\tan\beta = 2$ and $\tan\beta = 40$ are shown in figure 6. The limit obtained with the $\tilde{\chi}^{\pm} \to \tau^{\pm}J$ search is substantially better than the LEP1 limit [22].

6 Conclusion

Searches for spontaneous R-parity violating signals used a data sample of about $211\,\mathrm{pb}^{-1}$ collected by the DELPHI detector during 1997 and 1998 at centre-of-mass energies of 183 GeV and 189 GeV. In the present analysis it was assumed that the R-parity breaking occurs in the third generation and, as a consequence, the lightest chargino decays into a two-body decay mode $\tilde{\chi}^{\pm} \to \tau^{\pm} + J$. No evidence for R-parity spontaneously breaking has been observed, assuming a sneutrino mass above $300\,\mathrm{GeV/c^2}$.

In the search for $\tilde{\chi}^{\pm} \to \tau^{\pm} + J$, 15 candidates were selected, with 15.85 ± 0.59 expected from SM process. This allowed an upper limit on the chargino production cross-section of 0.23 pb and a lower limit on the chargino mass of $94.4\,\mathrm{GeV/c^2}$ to be obtained at 95% confidence level. The limit obtained with the present search is substantially better than the LEP1 limit [22].

7 Acknowledgements

We are greatly indebted to our technical collaborators, to the members of the CERN-SL Division for the excellent performance of the LEP collider, and to the funding agencies for their support in building and operating the DELPHI detector.
We acknowledge in particular the support of
Austrian Federal Ministry of Science and Traffics, GZ 616.364/2-III/2a/98,
FNRS–FWO, Belgium,
FINEP, CNPq, CAPES, FUJB and FAPERJ, Brazil,
Czech Ministry of Industry and Trade, GA CR 202/96/0450 and GA AVCR A1010521,
Danish Natural Research Council,
Commission of the European Communities (DG XII),
Direction des Sciences de la Matière, CEA, France,
Bundesministerium für Bildung, Wissenschaft, Forschung und Technologie, Germany,
General Secretariat for Research and Technology, Greece,
National Science Foundation (NWO) and Foundation for Research on Matter (FOM),

The Netherlands,
Norwegian Research Council,
State Committee for Scientific Research, Poland, 2P03B06015, 2P03B1116 and SPUB/P03/178/98,
JNICT–Junta Nacional de Investigação Científica e Tecnológica, Portugal,
Vedecka grantova agentura MS SR, Slovakia, Nr. 95/5195/134,
Ministry of Science and Technology of the Republic of Slovenia,
CICYT, Spain, AEN96–1661 and AEN96-1681,
The Swedish Natural Science Research Council,
Particle Physics and Astronomy Research Council, UK,
Department of Energy, USA, DE–FG02–94ER40817.

References

[1] H.P. Nilles, Phys. Rep. 110 (1984) 1.
H.E. Haber and G.L. Kane, Phys. Rep. 117 (1985) 75.

[2] C.S. Aulakh, R.N. Mohapatra, Phys. Lett. **B119** (1982) 136;
A. Santamaria, J.W.F. Valle, Phys. Lett. **B195** (1987) 423; Phys. Rev. Lett. **60** (1988) 397; Phys. Rev. **D39** (1989) 1780.

[3] J.W.F. Valle, Phys. Lett. **B196** (1987) 157;
M.C. Gonzalez-Garcia and J.W.F. Valle, Nucl. Phys. **B355** (1991) 330.

[4] A. Masiero and J.W.F. Valle, Phys. Lett. **B251** (1990) 273;
J.C. Romão, C.A. Santos and J.W.F. Valle, Phys. Lett. **B288** (1992) 311.

[5] F. de Campos, O.J.P. Éboli, M.A. García-Jareño, J.W.F. Valle, Nucl. Phys. **B546** (1999) 33.

[6] P. Nogueira, J.C. Romão, J.W.F. Valle, Phys. Lett. **B251** (1990) 142;
R. Barbieri, D.E. Brahm, J. Hall, S.D.H. Hsu, Phys. Lett. **B238** (1990) 86.

[7] J.C. Romão, J. Rosiek and J.W.F. Valle, Phys. Lett. **B351** (1995) 497;
J.C. Romão, N. Rius and J.W.F. Valle, Nucl. Phys. **B363** (1991) 369.

[8] R.N. Mohapatra and J.W.F. Valle, Phys. Rev. **D34** (1986) 1642;
J.W.F. Valle, Nucl. Phys. **B11**(Proc. Suppl.) (1989) 118.

[9] R. Barbieri, S. Ferrara and C.A. Savoy, Phys. Lett. **B119** (1982) 343.

[10] J.C. Romão and J.W.F. Valle, Phys. Lett. **B272** (1991) 436, Nucl. Phys. **B381** (1992) 87.

[11] J.C. Romão, A. Ioannissyan and J.W.F. Valle, Phys. Rev. **D55** (1997) 427,
M.A. Diaz, J.C. Romão and J.W.F. Valle, Nucl. Phys. **B524** (1998) 23.

[12] P.Aarnio *et al.*, Nucl. Instr. and Meth. **A303** (1991) 233;
P.Abreu *et al.*, Nucl. Instr. and Meth. **A378** (1996) 57.

[13] T. Sjöstrand; Computer Physics Communications **39** (1986) 347.

[14] S. Jadach, B.F.L. Ward and Z. Was; Computer Physics Communications **79** (1994) 503.

[15] J.E. Campagne and R. Zitoun, Zeit. Phys. **C43** (1989) 469.

[16] F.A. Berends, R. Kleiss, R. Pittau, Computer Physics Communications **85** (1995) 437.

[17] M. Böhm, A. Denner and W. Hollik, Nucl. Phys. **B304** (1988) 687;
F.A. Berends, R. Kleiss and W. Hollik, Nucl. Phys. **B304** (1988) 712.

[18] F.A. Berends, P.H. Daverveldt, R. Kleiss; Computer Physics Communications **40** (1986) 271, 285, 309.

[19] S. Nova, A. Olchevski, T. Todorov, "*A Monte Carlo event generator for two photon physics*", DELPHI note 90-35 PROG 152 (1990).

[20] P.Abreu *et al.*, Phys. Lett. **B372** (1996) 172.

[21] R.M. Barnett *et al.*, Phys. Rev. **D54** (1996).

[22] K. Mönig, "*Model independent limit of the Z-decays Width into Unknown particles*", DELPHI note 97-174 PHYS 748 (1997);
M. Acciari *et al.*, Phys. Lett. **B350** (1995) 109;
G. Alexander *et al.*, Phys. Lett. **B377** (1996) 273.

Centre-of-mass Energy	**183 GeV**	**189 GeV**
Observed events	**6**	**9**
Total background	**6.28 ± 0.40**	**9.55 ± 0.44**
$Z/\gamma \to ee, \mu\mu, \tau\tau, q\bar{q}$	0.86 ± 0.23	0.57 ± 0.12
4-fermion events except WW	0.60 ± 0.05	1.20 ± 0.16
$\gamma\gamma \to ee, \mu\mu, \tau\tau$	0.28 ± 0.13	0.21 ± 0.21
W^+W^-	4.38 ± 0.28	7.57 ± 0.33

Table 1: Chargino candidates with the total number of background expected and the contributions from major background sources at centre-of-mass energies of 183 GeV and 189 GeV. The errors quoted on the background correspond to the statistics uncertainties.

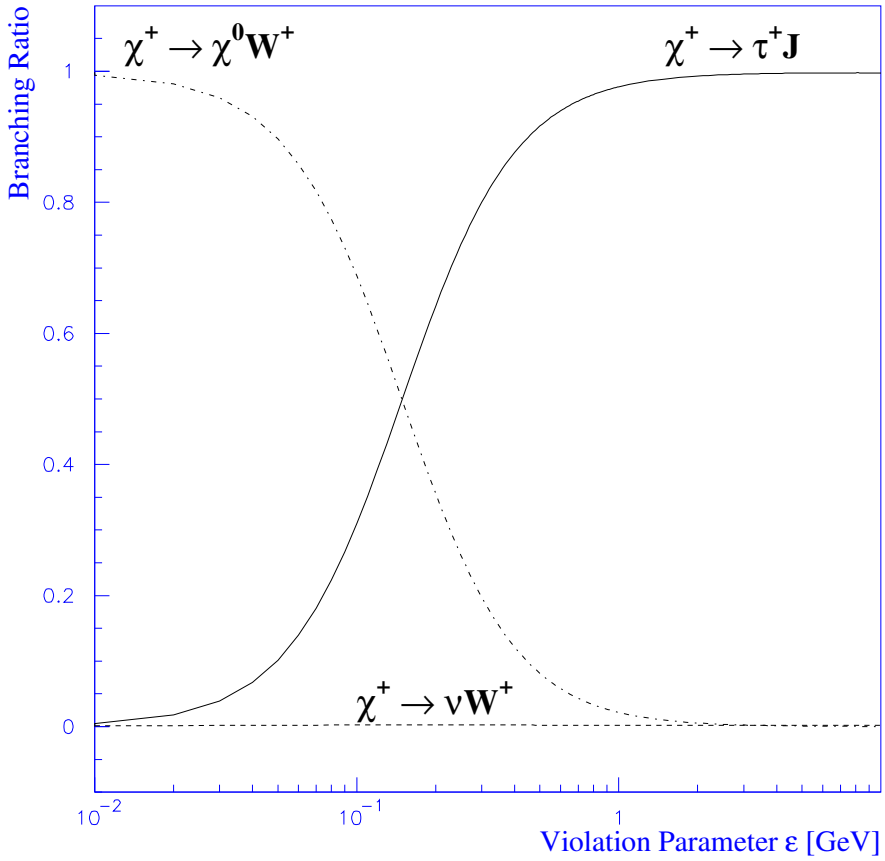

Figure 1: Chargino decay branching ratios as a function of the effective violation parameter, ϵ, at 189 GeV for $\tan\beta = 2$, $\mu = 100$ and $M_2 = 400$.

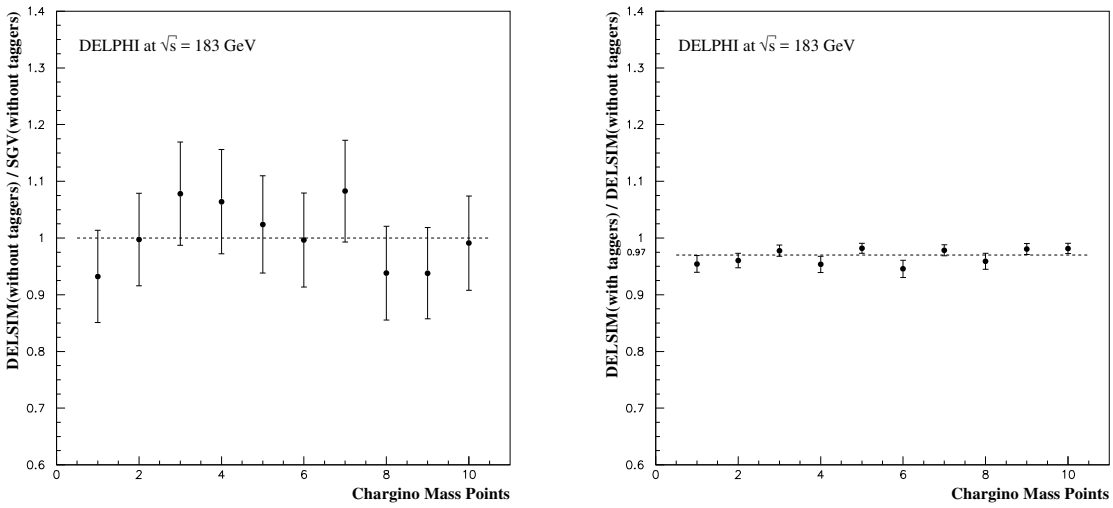

(a) (b)

Figure 2: Efficiency correction factors for SGV simulated signals. (a) Selection efficiency ratio between the DELSIM simulated events and the SGV simulated events, if the taggers are not considered in the DELSIM simulated events. (b) Ratio between the selection efficiencies for the DELSIM simulated events with and without the tagger cut. The dashed line shows the average value for the efficiency correction factor that is equal to 1, if we compare DELSIM and SGV efficiencies (a) and equal to 0.97, if we use the tagger cut for the DELSIM simulated events (b).

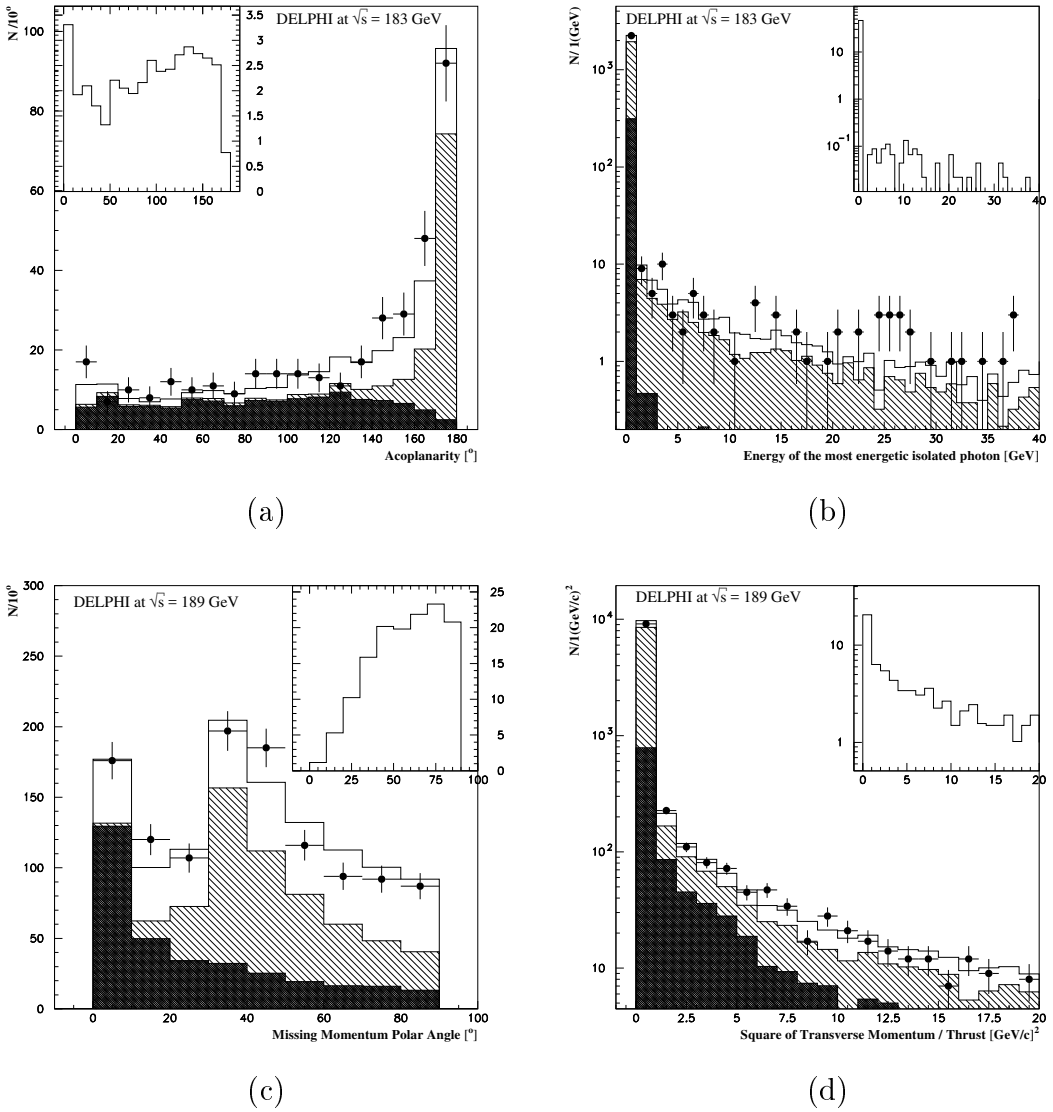

Figure 3: Distribution of (a) acoplanarity, (b) energy of the most energetic isolated photon, (c) angle between the missing momentum and the beam-axis and (d) square of transverse momentum with respect to the thrust axis divided by the thrust, after the preliminary selection described in the first paragraph of Section 4. For the acoplanarity and missing momentum polar angle distributions it was also required that the square of the transverse momentum with respect to the thrust axis divided by the thrust was above $0.75\,(\mathrm{GeV/c})^2$ and above $1\,(\mathrm{GeV/c})^2$, respectively. The points with error bars show the real data, while the white histogram show the total simulated background. The distributions corresponding to the $\gamma\gamma$ background and the Bhabha scattering are shown as dark and hatched histograms, respectively. An example of the two body decay mode $\tilde{\chi}^{\pm} \to \tau^{\pm} + J$ behaviour for $\tan\beta = 2$, $\mu = 100$ and $\mathrm{M}_2 = 400$ is shown in the upper plots for each variable.

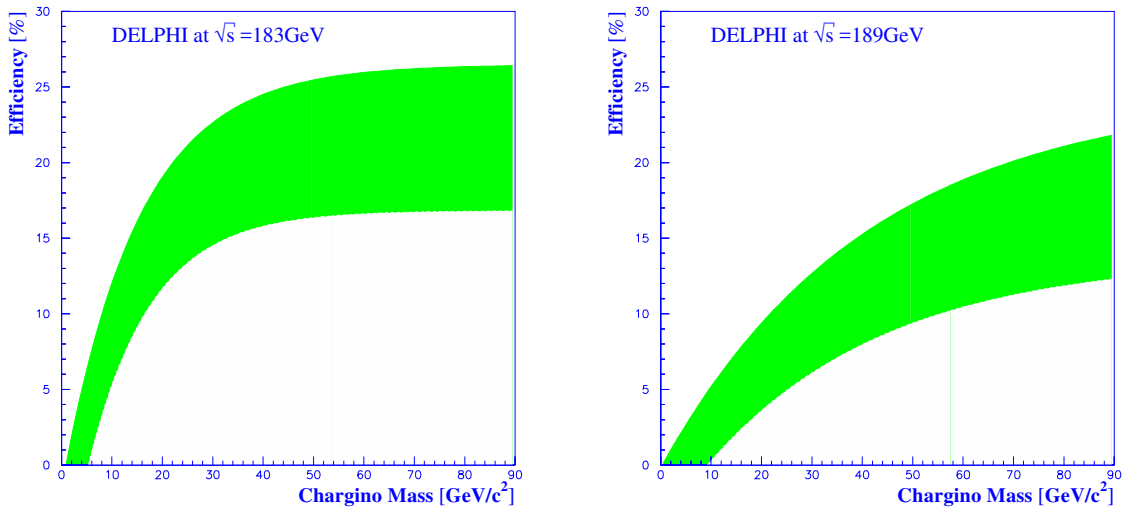

(a) (b)

Figure 4: Chargino detection efficiency as a function of the chargino mass for (a) 183 GeV and (b) 189 GeV of centre-of-mass energies, considering only the two body decay mode $\tilde{\chi}^{\pm} \to \tau^{\pm} + J$. The bands correspond to the statistical uncertainties combined with the effect of generating points with different MSSM parameters M_2 and μ, which have been varied in the ranges $40\ \mathrm{GeV/c^2} \leq M_2 \leq 400\ \mathrm{GeV/c^2}$ and $-200\ \mathrm{GeV/c^2} \leq \mu \leq 200\ \mathrm{GeV/c^2}$, for $\tan\beta = 2$.

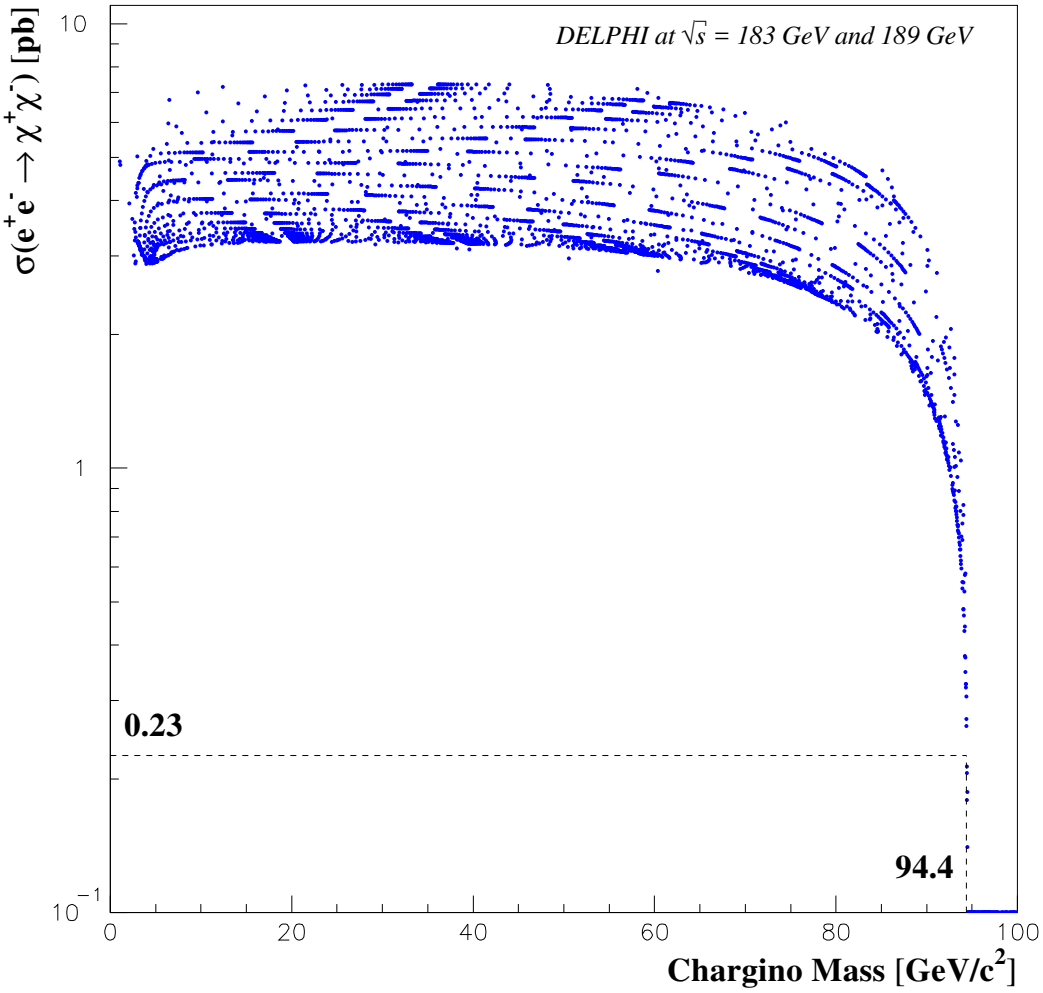

Figure 5: Expected $e^+e- \rightarrow \tilde{\chi}^+\tilde{\chi}^-$ cross-section at 189 GeV (dots) as a function of chargino mass, assuming a heavy sneutrino ($M_{\tilde{\nu}} \geq 300\,\mathrm{GeV/c^2}$). The dots correspond to the generating points at different chargino masses for the MSSM parameters ranges: $40\,\mathrm{GeV/c^2} \leq \mathrm{M_2} \leq 400\,\mathrm{GeV/c^2}$, $-200\,\mathrm{GeV/c^2} \leq \mu \leq 200\,\mathrm{GeV/c^2}$ and $2 \leq \tan\beta \leq 40$. At 95% confidence level assuming the chargino decays exclusively to $\tau^{\pm}J$, the minimal chargino production cross-section in the excluded mass region is 0.23 pb and the corresponding mass limit is $94.4\,\mathrm{GeV/c^2}$.

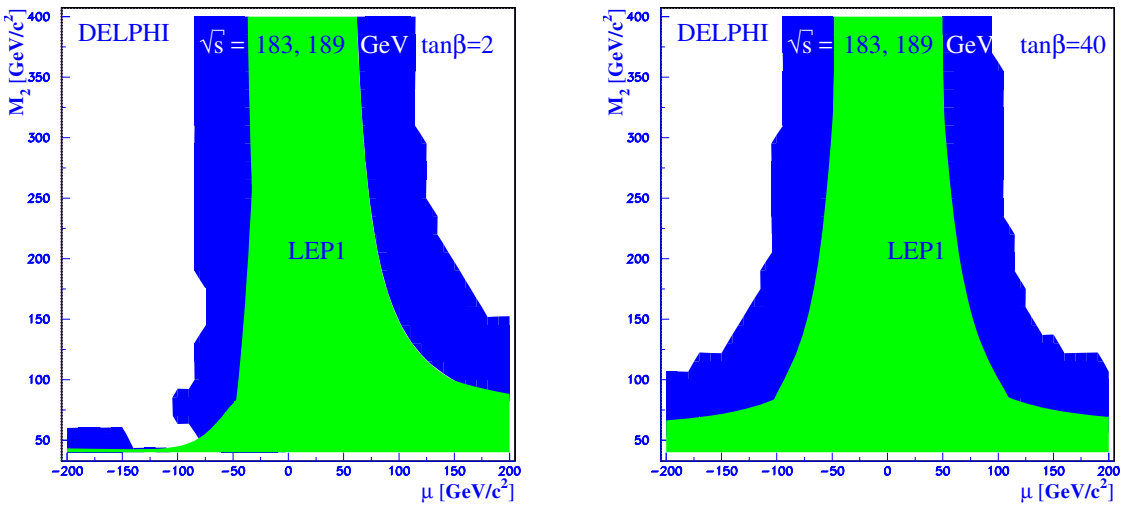

(a) (b)

Figure 6: Excluded regions in μ, M_2 parameter space at 95% confidence level for (a) $\tan\beta = 2$ and (b) $\tan\beta = 40$, assuming $M_{\tilde{\nu}} \geq 300\,\mathrm{GeV/c^2}$. The exclusion area obtained with the $\tilde{\chi}^{\pm} \to \tau^{\pm} J$ search is shown in dark grey and the corresponding area excluded by the LEP1 data[22] is shown in light grey. The hole seen on plot (a) around $M_2 = 50\,\mathrm{GeV/c^2}$ and $\mu = -120\,\mathrm{GeV/c^2}$ is due to the low branching ratio (below 5%) for the $\tilde{\chi}^{\pm} \to \tau^{\pm} J$.